



**HAL**  
open science

# Unraveling the Mechanism of Cysteine Persulfide Formation Catalyzed by 3-Mercaptopyruvate Sulfurtransferases

Jean-Christophe Lec, Séverine Boutserin, Hortense Mazon, Guillermo Mulliert, Sandrine Boschi-Muller, François Talfournier

► **To cite this version:**

Jean-Christophe Lec, Séverine Boutserin, Hortense Mazon, Guillermo Mulliert, Sandrine Boschi-Muller, et al. Unraveling the Mechanism of Cysteine Persulfide Formation Catalyzed by 3-Mercaptopyruvate Sulfurtransferases. *ACS Catalysis*, 2018, 8 (3), pp.2049-2059. 10.1021/acscatal.7b02432 . hal-01715178

**HAL Id: hal-01715178**

**<https://hal.univ-lorraine.fr/hal-01715178>**

Submitted on 28 Jan 2022

**HAL** is a multi-disciplinary open access archive for the deposit and dissemination of scientific research documents, whether they are published or not. The documents may come from teaching and research institutions in France or abroad, or from public or private research centers.

L'archive ouverte pluridisciplinaire **HAL**, est destinée au dépôt et à la diffusion de documents scientifiques de niveau recherche, publiés ou non, émanant des établissements d'enseignement et de recherche français ou étrangers, des laboratoires publics ou privés.

# Unraveling the mechanism of cysteine persulfide formation catalyzed by 3-mercaptopyruvate sulfurtransferases

*Jean-Christophe Lec,<sup>†</sup> Séverine Boutserin,<sup>†</sup> Hortense Mazon,<sup>†</sup> Guillermo Mulliert,<sup>‡</sup> Sandrine Boschi-Muller,<sup>\*†</sup> and François Talfournier<sup>\*†</sup>*

<sup>†</sup> Ingénierie Moléculaire et Physiopathologie Articulaire (IMoPA), UMR 7365 CNRS-Université de Lorraine, Bâtiment Biopole, Faculté de Médecine, Vandoeuvre-lès-Nancy, 54506, France

<sup>‡</sup> Cristallographie, Résonance Magnétique et Modélisations (CRM2), UMR 7036 CNRS-Université de Lorraine, Vandoeuvre-lès-Nancy, 54506, France

\* Co-corresponding authors

## ABSTRACT

Sulfhydration of reactive cysteines in target proteins is now recognized as a major route by which H<sub>2</sub>S mediates signal transduction and regulates various cellular processes. Among the enzymatic systems permitting the formation of cysteine persulfide from non-activated sulfur compounds, 3-mercaptopyruvate sulfurtransferases can be considered as a model of thiolate-based chemistry for carbon-sulfur bond breaking. These ubiquitous enzymes transfer a sulfur atom from 3-mercaptopyruvate (3-MP) to a thiol acceptor *via* a cysteine-persulfide intermediate, but the mechanistic basis for its formation is still unclear. To address this question, kinetic approaches were developed for studying the reaction catalyzed by the human and *Escherichia coli* enzymes and the role of several conserved residues was also investigated. We showed that the first step of sulfur transfer that leads to pyruvate release and formation of the persulfide intermediate is very efficient for both enzymes. It critically depends on the electrostatic contribution provided by the CGSGVT catalytic loop while any role of the so-called Ser/His/Asp triad can be excluded. Furthermore, solvent kinetic isotopic effect and proton inventory studies revealed a concerted mechanism in which the water-mediated protonation of the pyruvate enolate and the S<sup>0</sup> transfer from the deprotonated 3-MP to the thiolate form of the catalytic cysteine occurs concomitantly.

**KEYWORDS.** H<sub>2</sub>S signaling, 3-mercaptopyruvate sulfurtransferase, persulfide, active site electrostatics, mechanism, kinetics, catalysis

## INTRODUCTION

Over the past decade, increasing attention has been paid to persulfide (RSSH) chemistry due to the physiological functions ascribed to these entities, in particular in H<sub>2</sub>S-mediated redox signaling. Formation of protein-bound persulfides is a posttranslational modification that is thought to be involved in signal transduction although the mechanism behind S-sulfhydration remains unclear.<sup>1</sup> The high reactivity of RSSHs make them good sulfur donors, and explain why reactive cysteine persulfides formed in proteins are proposed to be key actors in H<sub>2</sub>S signaling pathways.<sup>2-6</sup>

*In vivo*, the formation of cysteine persulfides is achieved by two mechanisms. The first one consists in a reaction between an activated form of sulfur, H<sub>2</sub>S (HS<sup>-</sup> under physiological conditions), and an oxidized cysteine under disulfide or sulfenic acid form (Scheme 1).<sup>7,8</sup> The second mechanism involves non-activated sulfur compounds and thus requires an enzymatic catalysis. If a carbon-sulfur bond must be broken this is mainly achieved by the cysteine desulfurases and the 3-mercaptopyruvate sulfurtransferases (3-MSTs) (Scheme 2).<sup>1,2,9,10</sup> Cysteine desulfurases are pyridoxal 5'-phosphate (PLP)-dependent enzymes that catalyze the conversion of cysteine to alanine and sulfide *via* the formation of a reductively labile enzyme cysteinyl persulfide intermediate.<sup>11,12</sup>

By contrast, the 3-MSTs do not require cofactors and these ubiquitous enzymes that are involved in H<sub>2</sub>S production, belong to the rhodanese structural family.<sup>13,14</sup> The rhodanese domain displays a typical  $\alpha/\beta$  topology with a central five-stranded  $\beta$ -sheet flanked by four or five  $\alpha$ -helices.<sup>15,16</sup> In the X-ray structures available to date, the catalytic cysteine is mainly present at the persulfide state that is thought to be a key intermediate in the 3-MST-catalyzed reaction.<sup>17,18</sup> The catalytic mechanism of 3-MSTs is assumed to occur *via* two successive steps. The reaction is initiated by

the nucleophilic attack of the thiolate group of the catalytic cysteine on the sulfur atom of the donor substrate leading to formation of a persulfide intermediate on the catalytic cysteine and product release (Scheme 3). This intermediate then undergoes a nucleophilic attack by an acceptor substrate. If the latter is a thiol compound, the decomposition of the product formed leads to H<sub>2</sub>S production.<sup>14,18,19</sup> Based on the X-ray structure of *Leishmania major* 3-MST, the mechanism of persulfide formation is proposed to involve a serine protease-like catalytic triad, where the Ser239 acts as a base catalyst to activate the catalytic Cys237 and contributes to the stabilization of the transition state<sup>17</sup> (In this paper, the numbering of conserved amino acids refers to the *Escherichia coli* 3-MST (<sup>Ec</sup>3-MST) sequence missing the N-terminal Met, Figure S1).<sup>18</sup> Steady-state analyses performed on the R178G and R187G 3-MSTs from rat suggest that Arg178 must be important for the 3-mercaptopyruvate (3-MP) binding.<sup>20</sup> This statement is further supported by the structure of the human 3-MST (<sup>h</sup>3-MST) / pyruvate complex, in which both Arg178 and Arg187 hydrogen-bonded the carboxylate of the pyruvate while Arg187 additionally interacted with the carbonyl function (Figure 1).<sup>18</sup> Moreover, from the *E. coli* 3-MST structure, His66 and Arg102 are proposed to stabilize the 3-MP through hydrogen bond and electrostatic interaction, respectively.<sup>21</sup> Finally, very recent theoretical studies using QM/MM methods argue for a mechanism of persulfide formation in which the sulfur atom transfer is initiated by the deprotonation of 3-MP.<sup>22</sup> Nonetheless, it remains to be proven whether the cysteine persulfide intermediate is kinetically relevant to the 3-MST catalytic pathway and the molecular/mechanistic features responsible for its formation are still to be identified.

To address this gap in knowledge, we developed kinetic approaches for studying each step of the reaction catalyzed by two members of the 3-MST family (i.e. <sup>Ec</sup>3-MST and <sup>h</sup>3-MST) and defining the role of conserved residues in persulfide formation. Here, we propose a detailed

catalytic mechanism that emphasizes the critical electrostatic contribution of the CGSGVT active site loop and the requirement for a water-mediated protonation of the enolate pyruvate to permit an efficient first step of sulfur transfer.

## EXPERIMENTAL PROCEDURES

**Materials** – Commercial sodium salt of 3-MP (Santa Cruz Biotechnology) was further purified by reverse phase chromatography on a Delta-Pak C18 preparative column (19/300, Waters) coupled to an Aktä Explorer system (GE Healthcare) and equilibrated with 50 mM ammonium acetate buffer, pH 6.8. 3-MP was eluted isocratically before H<sub>2</sub>S/HS<sup>-</sup> and lyophilized before storage at -20°C. Lactate Dehydrogenase (LDH) and pyruvate were purchased from Sigma-Aldrich whereas NADPH and NADH were purchased from Roche. *E. coli* Trx1 and Trx reductase were prepared following experimental procedures already published.<sup>23,24</sup> The *3mst* ORFs were amplified from genomic DNA of *E. coli* DH5 $\alpha$ , or sourced from BioScience lifeScience for the synthetic human *3mst* ORF.

**Production and purification of <sup>h</sup>3-MST and <sup>Ec</sup>3-MST** – The *3mst* ORF from *E. coli* was amplified by PCR and the resulting fragment was first ligated into pCR-Blunt II and then into the *Nde*I-*Sac*I site of pET20b(+) (Novagen), generating pET20-<sup>Ec</sup>3MST. The synthetic human *3mst* ORF was ligated into the *Nde*I-*Sac*I site of pET28b(+) (Novagen), generating pET28-<sup>h</sup>3MST. Site-directed mutageneses were performed using the Quick Change site-directed mutagenesis kit (Stratagene). The recombinant plasmids were transformed into *E. coli* strain C41 (DE3) or BL21 (DE3) for inducible expression of untagged <sup>Ec</sup>3-MST or N-terminal His-tagged <sup>h</sup>3-MST, respectively. Freshly grown overnight cultures of *E. coli* C41 (DE3) or BL21 (DE3) cells were

used to inoculate LB supplemented with 200 mg/L ampicillin or 0.5 mg/L kanamycin for pET20- or pET28-plasmids, respectively. The cultures were incubated at 37 °C until  $A_{600}$  reached 0.8 then 1 mM iso-propyl- $\beta$ -D-thiogalactopyranoside was added. Following incubation at 20 °C for 18 h, the cells were harvested by centrifugation at 3000g for 20 min at 4 °C. At this stage, the cell pellets were used immediately for purification or washed with a buffer (50 mM Tris-HCl, 5 mM EDTA, 25% sucrose, pH 8.0) before storage at -20 °C.

For  $^h3$ -MST purification, the cell pellets were suspended in A-Ni buffer (50 mM Tris-HCl, 100 mM KCl, 40 mM imidazole, pH 8.0) containing 8 U/mL of Benzonase (Merck) and 4 mM  $MgSO_4$ , and sonicated. The supernatant was loaded onto a Ni NTA-agarose column equilibrated with A-Ni buffer using an Äkta Avant system (GE Healthcare). After being washed with equilibration buffer, the enzyme was eluted at 200 mM imidazole from a linear gradient ranging from 40 mM to 1 M in B-Ni buffer (50 mM Tris-HCl, 100 mM KCl, 1M imidazole, pH 8.0). Purified fractions were identified by 12.5% SDS-PAGE then pooled and dialyzed overnight against TE buffer (50 mM Tris-HCl, 2 mM EDTA, pH 8.0). For  $^{Ec3}$ -MST purification, the cell pellets were suspended in TE buffer containing 8 U/mL of Benzonase (Merck) and 4 mM  $MgSO_4$ , and sonicated. The enzyme was then precipitated at 65%  $(NH_4)_2SO_4$  saturation and after centrifugation the pellet was suspended in TE buffer containing 1 M  $(NH_4)_2SO_4$ . The enzymatic solution was applied onto a Phenyl-Sepharose column previously equilibrated with TE buffer containing 1 M  $(NH_4)_2SO_4$  using an Äkta Avant system (GE Healthcare). After washing with equilibration buffer, the enzyme was eluted at 650 mM  $(NH_4)_2SO_4$  using a descending gradient (1 to 0 M) of  $(NH_4)_2SO_4$ . Purified fractions were then pooled, diluted in TE buffer and applied to a Q-Sepharose column equilibrated with TE buffer.  $^{Ec3}$ -MST was eluted at 600 mM KCl using a 0-1 M KCl gradient.

At this stage, all enzymes were purified to homogeneity as estimated by 12.5% SDS–PAGE. The yield was approximately 30 and 100 mg of <sup>h</sup>3-MST and <sup>Ec</sup>3-MST per liter of culture, respectively, and the molecular masses of  $35210.4 \pm 0.4$  and  $30680.6 \pm 0.3$  Da determined by mass spectrometry under denaturing conditions were in good agreement with the 35210.5 and 30680.6 Da predicted from the <sup>h</sup>3-MST and <sup>Ec</sup>3-MST sequence, respectively. Purified enzymes were stored at  $-20$  °C in the presence of 10 mM DTT and 70% (NH<sub>4</sub>)<sub>2</sub>SO<sub>4</sub>. Under these conditions, the enzymes were stable for several months. Enzyme concentrations were determined spectrophotometrically, using molar absorption coefficients at 280 nm of 51350 and 51907 M<sup>-1</sup>.cm<sup>-1</sup> for <sup>h</sup>3-MST and <sup>Ec</sup>3-MST, respectively.

***Steady-state kinetic studies*** – Steady-state kinetic parameters were determined at 30 °C in TE buffer with saturated or variable concentrations of 3-MP and *E. coli* Trx1 in the presence of a Trx-regenerating system (1.25 μM *E. coli* Trx reductase (TrxR) and 0.3 mM NADPH). The concentration of enzyme was 0.01 μM and 1 μM for the <sup>Ec</sup>3-MST and <sup>h</sup>3-MST, respectively, and initial rate measurements were carried out on a SAFAS UVmc<sup>2</sup> spectrophotometer by following the oxidation of NADPH at 340 nm. Data were fit to the Michaelis-Menten equation or the Hill equation using least-squares regression analysis (SigmaPlot 2000, Jandel Scientific) to determine

$k_{\text{cat}}$ ,  $K_M$  or  $K_{0.5}$  and Hill number (n) values with  $k_{\text{cat}} = \frac{k_2.k_3.k_5.k_6}{k_3.k_5.k_6+k_2.k_5.k_6+k_2.k_3.k_6+k_2.k_3.k_5}$  (Scheme 4B).

***Fluorescence properties of 3-MSTs*** – The fluorescence excitation and emission spectra of 3-MSTs in their reduced and persulfide states were recorded on a Xenius spectrofluorometer (SAFAS) equipped with a temperature controlled stirred cell. All measurements were performed at 30 °C using 10 μM of enzyme in TE buffer. The persulfide forms were obtained by mixing

reduced 3-MSTs with a 5-fold excess of 3-MP during 5 minutes, followed by passing the solution through a PD Mini-Trap G-25 column (GE Healthcare). The excitation wavelength was set to 287 nm to record emission spectra from 300 to 400 nm, whereas the emission wavelength was set to 330 and 335 nm to obtain excitation spectra from 240 to 310 nm for <sup>h</sup>3-MST and <sup>Ec</sup>3-MST, respectively.

***Single turn-over experiments*** – Except for quenched-flow experiments, all single turn-over studies were carried out on an SX19MV-R stopped flow apparatus (Applied PhotoPhysics), and collected data were analyzed using the SX19MV-R software package.

***Determination of the rate of pyruvate formation*** – Rapid chemical quench experiments were carried out at 30 °C on a KinTek RFQ-3 instrument (KinTek Corporation). Under the conditions used, a minimum ageing time of about 2.5 ms was determined. Equal volumes of a solution containing 430 µM of 3-MST in TE buffer and a solution containing 4 mM 3-MP in TE buffer were mixed and allowed to react for 2.5 ms to 10 s before being quenched with an equal volume of an aqueous solution containing 9 % of perchloric acid. Quenched samples were collected and then analysed. After centrifugation, pyruvate quantification in the resulting supernatant was carried out by reverse phase chromatography: 100 µL were injected onto a 4.6 x 250 mm C18 column Atlantis (Waters) coupled to an Aktä Explorer system (GE Healthcare) equilibrated with 50 mM phosphate buffer, pH 2.0. Pyruvate was eluted isocratically before 3-MP and quantified by peak integration at 215 nm and using the calibration curve equation (Area = 0.36 x [pyruvate] + 6.42) established with variable concentrations of pyruvate (25-500 µM). The concentration of pyruvate was plotted against time and fit to equation 1:

$$[\text{Pyruvate}] = A \cdot (1 - e^{-k_{\text{obs}} \cdot t}) + b \cdot t + c \quad (\text{Eq.1})$$

where A is the total concentration of pyruvate formed,  $k_{\text{obs}}$  is the observed rate constant, b is the slope of the linear phase, and c is the endpoint.

Kinetics of persulfide 3-MST formation – Kinetics of Trp fluorescence decrease associated with the formation of the persulfide 3-MST were measured at 30 °C. The excitation wavelength was set at 295 nm and the emitted light was detected using a 320 nm cut-off filter. One syringe was filled with 3-MST in TE buffer (10  $\mu\text{M}$  final concentration after mixing) and the other contained 3-MP at various concentrations. An average of at least five runs was recorded for each substrate concentration and collected data were fit to a biphasic expression (single exponential + slope) where the first kinetic phase represents the fast decrease in fluorescence accompanying the reduced-persulfide transition. The resulting  $k_{\text{obs}}$  data were fit to equation 2 to determine  $k_{\text{max1}}$  and  $K_{3\text{-MP}}$ , the apparent affinity constant for 3-MP.

$$k_{\text{obs}} = k_{\text{max1}} \cdot [\text{S}] / (K_{3\text{-MP}} + [\text{S}]) \quad (\text{Eq.2})$$

with  $k_{\text{max1}} = k_2$  and  $K_{3\text{-MP}} = \frac{k_{-1} + k_2}{k_1}$  (Scheme 4B).

For wild-type and H66A <sup>h</sup>3-MSTs, the pH dependence of the rate constant  $k_{\text{max1}}$  was studied at 30 °C over a pH range 4.0–10.0 in polybuffer A containing 30 mM acetic acid, 30 mM imidazole, 120 mM Tris/HCl at constant ionic strength of 0.15 M in the presence of a saturating concentration of 3-MP.  $k_{\text{max1}}$  values were plotted against pH and fit to equation 3, deriving from a one-pKa model, where  $k_{\text{lim}}$  represent the maximum pH-independent rate constant.

$$k_{\text{max1}} = \frac{k_{\text{lim}}}{(1 + 10^{(pK_a - pH)})} \quad (\text{Eq.3})$$

Kinetics of sulfur transfer from the persulfide 3-MST to Trx – Kinetics of sulfur transfer from the persulfide 3-MST to Trx were measured at 30°C with the Trx-regenerating system by following the oxidation of NADPH at 340 nm. Persulfide 3-MST was pre-formed as described in the paragraph *Fluorescence properties of 3-MSTs*. One syringe contained persulfide 3-MST (1-10  $\mu\text{M}$ )

and TrxR (37.5  $\mu\text{M}$ ) in TE buffer and the other one contained NADPH (0.3 mM) and Trx at various concentrations in TE buffer. To eliminate the background due to the NADPH oxidase activity of TrxR, control experiments were done under the same experimental conditions but in the absence of 3-MST, and the resulting transients were subtracted from those obtained in the presence of persulfide 3-MST. An average of at least five runs was recorded for each substrate concentration and the progress curves were fit to double exponential expression: the first kinetic phase represents the reduction of disulfide Trx by TrxR, whereas the second reflects a side-reaction between TrxR and HS<sup>-</sup> generated concomitantly to disulfide Trx. Rate constants  $k_{\text{obs}}$  were obtained by fitting fluorescence traces to a double exponential expression and these data were fit to equation 4 to determine  $k_{\text{max}2}$  and  $K_{\text{Trx}}$ , the apparent affinity constant for Trx.

$$k_{\text{obs}} = k_{\text{max}2} \cdot [\text{S}] / (K_{\text{Trx}} + [\text{S}]) \quad (\text{Eq.4})$$

with  $k_{\text{max}2} = k_5$  and  $K_{\text{Trx}} = \frac{k_{-4} + k_5}{k_4}$  (Scheme 4B).

*Determination of dissociation rate constant for pyruvate* – The rate of pyruvate dissociation from the persulfide 3-MST/pyruvate binary complex was measured at 30 °C using the coupled pyruvate/LDH assay as a pyruvate-trapping system. One syringe was filled with 1.25  $\mu\text{M}$  LDH and 300  $\mu\text{M}$  NADH in TE buffer and the other contained 5  $\mu\text{M}$  pyruvate and 2.5  $\mu\text{M}$  persulfide 3-MST (or not for the control experiment), in TE buffer. Data were fit to a biphasic expression.

*Measurement of the thiol ionization by ultraviolet absorbance* – Absorbance spectra were measured for all enzymes in 1.0-cm path-length quartz cuvettes in a SAFAS UVmc<sup>2</sup> spectrophotometer. The proteins samples were diluted in polybuffer A and spectra were recorded at 30 °C in 0.5-nm steps from 200 nm to 300 nm. The buffer solution was scanned relative to air, followed by a protein solution in the same cuvette versus air. The two spectra were then subtracted

and the difference converted to molar absorption coefficients at 240 nm ( $\epsilon_{240\text{ nm}}$ ). Data were fit to a one-pKa model,

$$\epsilon_{240\text{ nm}} = \epsilon_{\text{SH}} + \frac{\epsilon_{\text{S}^-} - \epsilon_{\text{SH}}}{1 + 10^{(\text{pKa} - \text{pH})}} \quad (\text{Eq.5})$$

where  $\epsilon_{\text{SH}}$  and  $\epsilon_{\text{S}^-}$  are the molar absorption coefficients of the thiol and the thiolate species, respectively.

***Solvent kinetic isotope effect and proton inventory experiments*** – The <sup>h</sup>3-MST and the 50 mM Tris buffer were lyophilized and redissolved in D<sub>2</sub>O and the 3-MP was freshly prepared in D<sub>2</sub>O. The pD of the reconstituted D<sub>2</sub>O buffer was checked with a conventional glass electrode and the observed pH reading was corrected using the relationship pD = observed pH-meter reading + 0.4.

<sup>25</sup> The  $k_{\text{max1}}$  values were determined under single turn-over conditions at saturating 3-MP concentration (1 mM) and pL 8.0 (L= H or D). The solvent kinetic isotope effect (SKIE) was given by the ratio of the rate constant  $k_{\text{max1}}$  obtained in pure H<sub>2</sub>O ( $k_0$ ) and that obtained in D<sub>2</sub>O ( $k_{\text{D}_2\text{O}}$ ). For proton inventory, the fraction of D<sub>2</sub>O was varied from 0 to 100 % (i.e.  $0 \leq n \leq 1$ ). In each case,  $k_{\text{max1}}$  values were determined under similar conditions to that described above. Data were analyzed by plotting the ratio of the rate constant  $k_n$  obtained at a particular D<sub>2</sub>O fraction (n), and the rate constant  $k_0$  obtained in pure H<sub>2</sub>O versus n. The points were fit to the simplified Gross-Butler equation:<sup>25</sup>

$$k_n/k_0 = 1 - n + n \cdot \Phi^T \quad (\text{Eq.6})$$

where  $\Phi^T$  is the inverse SKIE.

## RESULTS / DISCUSSION

***Steady-state kinetics for the wild-type 3-MSTs*** –The steady-state kinetic parameters were determined in the presence of 3-MP and Trx as donor and acceptor substrates, respectively, using TrxR and NADPH as a coupled assay. Although both enzymes displayed similar  $K_M$  values, the  $k_{cat}$  was 238-fold higher for  $E^c$ 3-MST (Table 1). Moreover, as previously reported by Banerjee and coll.,<sup>18</sup>  $h^3$ -MST exhibited kinetic cooperativity with respect to 3-MP and Trx. This behavior that may result from hysteresis<sup>18,26,27</sup> cannot be adequately described by a “classical” ping-pong mechanism (scheme 4B black parts). One possible explanation is the requirement for conformational transitions to occur between the two steps of sulfur transfer (scheme 4B grey parts), with E and E\* two conformations of the enzyme that are in equilibrium and catalytically competent for the first and the second step, respectively. Kinetic cooperativity would thus result from  $E_1^* \rightleftharpoons E_1$  and  $E_2 \rightleftharpoons E_2^*$  transitions not rapid enough to be at equilibrium during catalysis (i.e. with rate-constants comparable to  $k_{cat}$ ). One can postulate that our proposed kinetic scheme is also valid for the  $E^c$ 3-MST-catalyzed reaction but, in this case, the  $E_1^* \rightleftharpoons E_1$  and  $E_2 \rightleftharpoons E_2^*$  transitions are likely much faster than the catalytic cycle so that no kinetic cooperativity is revealed. Interestingly, under single turn-over conditions (see next parts), the absence of lag phase in the transient kinetics obtained for each step of sulfur transfer suggests that the E and E\* conformations are thermodynamically favored for the thiol and the persulfide form of the enzyme, respectively. Therefore, these additional E  $\rightleftharpoons$  E\* interconversion processes (scheme 4B grey parts) are no more relevant and the associated microscopic rate-constants can be ignored in the expression of the transient parameters  $K_{3-MP}$  and  $K_{Trx}$ . While the complete characterization of the reaction pathway is beyond the scope of the current study, this has to be pointed out because it could explain why the

values of  $k_{\max 1}/K_{3\text{-MP}}$  and  $k_{\text{cat}}/K_M$  (or  $k_{\text{cat}}/K_{0.5}$ ) that are expected to be similar for a ping-pong mechanism differ by several orders of magnitude (Table 1).

Because steady-state kinetics were not appropriate to investigate the catalytic mechanism of 3-MSTs and to elucidate the role of several conserved residues, in particular those of the so-called Ser-His-Asp triad in the first step of sulfur transfer, we developed experimental approaches to perform detailed kinetic studies on each step.

*The formation of the persulfide intermediate is very rapid for wild-type 3-MSTs* – As previously mentioned, the proposed mechanism for the 3-MSTs-catalyzed reaction is thought to proceed through the formation of a persulfide intermediate on the catalytic cysteine residue.<sup>18</sup> In that case, accumulation of this intermediate and concomitant formation of pyruvate should occur in the absence of acceptor substrate. This assumption was strongly supported by ESI-MS measurements performed on <sup>Ec</sup>3-MST before, and after incubation with 2 mM 3-MP under single turn-over conditions (i.e. without acceptor substrate), which revealed a 32 Da increase in the molecular mass of the enzyme upon 3-MP treatment (Figure S2). This also emphasized the stability of the persulfide intermediate within the 3-MSTs active site that could originate from several hydrogen bonds between the distal sulfur atom of the cysteinyl persulfide and neighbouring peptidic NH groups (Figure 1)<sup>18</sup>. Although our experimental data agreed well with the proposed two-step chemical mechanism (Scheme 3) it remained to be established whether the formation of a cysteine persulfide intermediate was kinetically relevant. To determine the rate constant associated with the formation of the persulfide intermediate, one possibility was to follow the concomitant formation of pyruvate. At various times of incubation of 3-MST with 2 mM 3-MP, in the absence of acceptor substrate, the reaction mixture was quenched with perchloric acid.

Pyruvate was then quantified by reverse-phase chromatography analysis and a burst of pyruvate production was observed (data not shown). Unfortunately, the rate constant was too high, at least  $1000\text{ s}^{-1}$ , to be accurately determined with the quenched-flow apparatus, which gave a minimum aging time of 2.5 ms. Therefore, we took advantage of the 40 % decrease in the fluorescence emission intensity of 3-MSTs upon going from the reduced to the persulfide forms (Figure S3). Following selective excitation of Trp residues at 295 nm, the change in fluorescence emission of 3-MSTs was thus measured under single turn-over conditions using a stopped-flow apparatus.

Irrespective of the 3-MP concentration, a fast decrease in the fluorescence emission signal was observed for both enzymes. Interestingly, this decrease was no longer detected in W10A<sup>Ec</sup>3-MST (data not shown), suggesting that invariant Trp-10 was a good probe to sense a change in the active site environment along the sulfur transfer process. Moreover, the fact that the rate-constants associated with the persulfide or the pyruvate formation were shown to be similar for H66A<sup>Ec</sup>3-MST (i.e.  $21.9 \pm 0.1\text{ s}^{-1}$  vs  $15 \pm 1\text{ s}^{-1}$  in the presence of 2 mM 3-MP, Figure 2A and 2B) further confirmed that monitoring the fluorescence change was an appropriate method for investigating the kinetics of the first step of sulfur transfer (step a scheme 4). Fast kinetic experiments were then carried out at pH 8 under single turn-over conditions in the absence of Trx. Saturation kinetics were obtained with respect to 3-MP and  $K_{3\text{-MP}}$  values of  $160 \pm 30$  and  $110 \pm 10\text{ }\mu\text{M}$  and  $k_{\text{max}1}$  values of  $1520 \pm 90$  and  $290 \pm 10\text{ s}^{-1}$  were determined for <sup>Ec</sup>3-MST and <sup>h</sup>3-MST, respectively (Figure 2C and 2D). These data indicated that the formation of the persulfide intermediate is rapid and not rate-limiting with  $k_{\text{max}1}$  values 13- and 617-fold higher than the  $k_{\text{cat}}$  values (Table 1). Therefore, the rate-limiting step of the reaction follows the persulfide intermediate/pyruvate complex formation and could be associated with pyruvate release or the second step of sulfur transfer (Scheme 4).

***The pyruvate dissociation is rate-limiting*** – The rate constant of pyruvate dissociation ( $k_{\text{off}}$ ) from the persulfide intermediate/pyruvate complex (step b scheme 4) was determined using LDH as a pyruvate-trapping system. The experiments were performed using <sup>h</sup>3-MST at pH 8 under single turn-over conditions in the absence of Trx. The resulting progress curves were fit to a biphasic expression: the first kinetic phase represents the reduction of unbound pyruvate, whereas the second corresponds to the titration of pyruvate that dissociates from the persulfide intermediate/pyruvate complex (Figure 3A, lower trace). Under the experimental conditions used, an apparent rate constant  $k_{\text{off}}$  of  $0.56 \text{ s}^{-1}$  was determined for the pyruvate release from the binary complex. Because  $k_{\text{off}}$  and  $k_{\text{cat}}$  values are similar ( $0.56 \text{ s}^{-1}$  vs  $0.47 \text{ s}^{-1}$ ), the rate-limiting step of the <sup>h</sup>3-MST-catalyzed reaction is associated with the pyruvate dissociation. Although it can be postulated that the same is true for <sup>Ec</sup>3-MST, this could not be validated experimentally. Indeed, the rate constant of  $1.52 \text{ s}^{-1}$  determined for pyruvate reduction by LDH (Figure 3A, upper trace) was approx. 70-fold lower than the rate constant associated with the pyruvate release that must be at least equal to  $112 \text{ s}^{-1}$  (i.e. the  $k_{\text{cat}}$  value for <sup>Ec</sup>3-MST) thus preventing the determination of the  $k_{\text{off}}$  value. However, an indirect validation rested on the determination of the rate constant associated with the second step of sulfur transfer.

In the presence of Trx as acceptor substrate, the sulfur transfer from the persulfide intermediate to Trx leads to reduction of 3-MST and to formation of a persulfide intermediate on the nucleophilic Cys32 from Trx, which rapidly evolves to generate the disulfide Trx and H<sub>2</sub>S.<sup>14</sup> Therefore, a convenient method to study the second step of sulfur transfer was to follow, under single turn-over conditions, the fluorescence increase associated with the persulfide-reduced transition undergone by 3-MSTs upon sulfur transfer to Trx. Unexpectedly, no fluorescence change was observed showing that the magnitudes of the fluorescence increase for 3-MSTs

reduction and fluorescence decrease for Trx oxidation were likely equal.<sup>28</sup> An alternative was to use the NADPH/Trx reductase as reporting system. However, one needs to bear in mind that such kinetics do not only reflect the second step of sulfur transfer but also the concomitant formation of disulfide Trx and H<sub>2</sub>S (step c scheme 4). Under the experimental conditions used, the rate constant for Trx reduction was 5-fold lower than the  $k_{\text{cat}}$  value determined for the <sup>Ec</sup>3-MST-catalyzed reaction (i.e. approx. 20 s<sup>-1</sup> vs 112 s<sup>-1</sup>, data not shown), thus precluding the use of this coupled assay for studying the kinetics of the bacterial enzyme. Fortunately, the picture differed for the human enzyme and experiments performed in the presence of 1-10 μM persulfide <sup>h</sup>3-MST and 10-250 μM Trx, yielded an apparent affinity constant  $K_{\text{Trx}}$  of  $24 \pm 5$  μM and a rate constant  $k_{\text{max}2}$  of  $2.3 \pm 0.2$  s<sup>-1</sup> which was 5-fold higher than the  $k_{\text{cat}}$  (Figure 3B). Together, our data showed that the two steps of sulfur transfer are catalytically efficient for both enzymes with rate constants ( $k_{\text{max}1}$  and  $k_{\text{max}2}$ ) ranging from 2.3 s<sup>-1</sup> to 1520 s<sup>-1</sup> (Table 1) and that H<sub>2</sub>S formation is fast as well. Moreover, pyruvate dissociation is shown to be rate-limiting, at least for the human enzyme, but is at least 200-fold faster for <sup>Ec</sup>3-MST. Although this remains to be explained at the molecular level, it may reveal significant differences in structural dynamics associated with catalysis between the human and the bacterial enzymes, such as the increased flexibility of the 61-67 and 181-198 regions in <sup>Ec</sup>3-MST that may strongly favor the release of pyruvate.<sup>21</sup>

***Effects of the Arg178L and Arg187L substitutions*** – The kinetic parameters determined at pH 8.0 are summarized in Table 1. Substituting Leu for each or both Arg residues resulted in a 4- to 15-fold increase in  $K_M$  for 3-MP and a 700- to 2200-fold decrease in  $k_{\text{cat}}$ . Although these drastic effects highlighted the critical role of both Arg178 and Arg187 residues in the 3-MST-catalyzed reaction, comparison of the  $k_{\text{max}1}$  and  $K_{3\text{-MP}}$  constants determined under single turn-over conditions

for the wild-type and the mutated 3-MSTs were expected to furnish additional insights into their role(s) in the first step of sulfur transfer. Interestingly, the 45- to 413-fold decrease in the  $k_{\max 1}/K_{3\text{-MP}}$  value reflects either a 72-fold decrease in  $k_{\max 1}$  or a 94-fold increase in  $K_{3\text{-MP}}$  for the R178L or the R187L 3-MSTs, respectively. Therefore, the role we can assign to each Arg differs to what was proposed by Yadav *et al.*, with a stabilization of the 3-MP binding ensured by the Arg187 side-chain through an interaction between the guanidinium group and the C3-carboxylate, while the Arg178 side-chain interacts with the C3-carboxylate and the C2-carbonyl functions to permit an efficient positioning of the 3-MP with respect to the catalytic Cys237. Our interpretation is strongly supported by the fact that the authors clearly indicate that the positions of the carboxyl and carbonyl groups in 3-MP or pyruvate are indistinguishable in the <sup>h</sup>3-MST crystalline binary complex.<sup>18</sup> As shown by the “moderate” decrease in  $k_{\max 1}/K_{3\text{-MP}}$ , the first step of sulfur transfer is not drastically impaired for both R178L and R187L 3-MSTs suggesting that the remaining Arg residue may compensate the absence of the other one. One can also postulate that additional contributions are likely to be critical for the catalytic efficiency of the first step because substituting both Arg does not fully abolish the sulfur transfer (Table 1,  $k_{\max 1}/K_{3\text{-MP}}$  3800-fold lower for R178L/R187L 3-MST). Finally, the rate-limiting step remains associated with the pyruvate release irrespective of the mutated Arg, with  $k_{\text{off}}$  values of 0.04 and 0.07 s<sup>-1</sup> for R178L and R187L 3-MSTs, respectively (curves not shown). This result is rather in agreement with our hypothesis regarding the role of the increased flexibility of the 181-198 loop in favoring the pyruvate release in <sup>Ec</sup>3-MST. Whether these substitutions restrict the mobility of this loop or modify its conformation remains to be evaluated, and in this respect, molecular dynamics experiments are expected to be informative.

***The Ser/His/Asp triad is not directly involved in catalysis*** – As shown in Table 1, substituting Ala for Ser239 in <sup>Ec</sup>3-MST led to a 45-fold decrease in  $k_{cat}$ , a 4-fold increase in  $K_{3-MP}$  but had no significant impact on  $k_{max1}$  value. Therefore, any key role of the Ser hydroxyl group in the persulfide formation can be excluded, in contrast to what was proposed in other studies.<sup>17,18</sup> This statement is further supported by the fact that the same substitution in the human enzyme is even more neutral with a 3-fold decrease in  $k_{cat}$ , no change in  $k_{max1}$  and an 8-fold increase in  $K_{3-MP}$ . Regarding the role of the His residue of the triad, substituting Ala for His66 in <sup>Ec</sup>3-MST did not significantly change the steady-state kinetic parameters with a 5.5-fold decrease in  $k_{cat}$ , but the first step of sulfur transfer became rate-limiting with a  $k_{max1}$  value 60-fold lower (Table 1). As expected, introducing at this position an Asn residue, that may restore the H-bond network established between the residues of the triad, increased the catalytic efficiency up to the wild-type level. Nevertheless, this network cannot be considered as essential for the formation of the persulfide because its loss only led to a 40-fold decrease in the  $k_{max1}/K_{3-MP}$  ratio. This hypothesis is strongly supported by the results obtained on the H66A <sup>h3</sup>-MST with a moderate 10-fold decrease in  $k_{max1}/K_{3-MP}$  ratio relative to the wild type and a rate-limiting step that remains associated to a process that follows the first step of sulfur transfer. However, the more obvious consequence of this substitution is the disappearance of the hysteric behavior observed for the wild type under steady-state conditions. The substitution of Asp53, the last conserved residue of the triad, into Ala did not change the kinetic parameters of <sup>Ec</sup>3-MST for the first step. This residue is thus not essential for the 3-MST-catalyzed persulfide formation. Finally, regardless of the 3-MST X-ray structures, the guanidinium group of invariant Arg102 appears to be H-bonded to the carbonyl functions of His66 and Gly240 (Figure 1). We thus hypothesized that Arg102 was indirectly involved in the catalysis of the first step by anchoring the loop that contains the catalytic Cys237. As shown in Table 1, the

$k_{\max 1}/K_{3\text{-MP}}$  ratio was 71- and 18-fold decreased for the R102L and R102K <sup>Ec</sup>3-MSTs, respectively, and for both enzymes the first step of sulfur transfer becomes rate-limiting as already observed for the H66A <sup>Ec</sup>3-MST. These results are rather consistent with our proposal because a bidentate interaction would account for the similar effects of both mutations on the catalysis. Additional support is also provided by the results obtained on the H66A/R102L <sup>Ec</sup>3-MST that revealed a cumulative effect of the substitutions with a 170-fold decrease in the  $k_{\max 1}/K_{3\text{-MP}}$  ratio that originates from a significant decrease in  $k_{\max 1}$ . Altogether this delineates a pattern of H-bond interactions that seems to be critical for stabilizing a conformation of the catalytic loop that is required for an efficient first step of sulfur transfer.

***The persulfide formation is mainly driven by electrostatic contributions provided by the catalytic loop*** – Another key question that needs to be addressed regarding the catalytic efficiency of the first step of sulfur transfer is the requirement for the Cys237 and the 3-MP thiol groups to be deprotonated. As we proposed a role for the peptidic NH groups of the so-called catalytic loop (CGSGVT loop, Figure 1) in the stabilization of the persulfide intermediate, they were also expected to lower the  $pK_{\text{app}}$  values of both –SH groups for increasing their chemical reactivity at neutral pH. Therefore, a disruption of the H-bond network that anchors this loop (see previous paragraph) was likely to modify the ionization state of both thiol groups, in particular that of the substrate. Because  $k_{\max 1}$  values remained in the same range (25 to 52 s<sup>-1</sup>) irrespective of the substitutions made (H66A and R102L/K for <sup>Ec</sup>3-MST or H66A <sup>h</sup>3-MST), we thus decided to perform pH-dependence studies on one of those mutants in addition to the wild type. Due to experimental reasons (see below), pH-dependence studies were carried out on the wild-type and H66A <sup>h</sup>3-MSTs. The ionization of the catalytic –SH group was selectively monitored on the free

<sup>h</sup>3-MST by the detection of the thiolate absorbance at around 240 nm (see e.g. <sup>29</sup>). To avoid any additional contribution of the polypeptidic chain in this wavelength region, the C237A or the C237A H66A mutant was used as internal reference for the wild-type or the H66A <sup>h</sup>3-MST, respectively. The pH/absorbance curves exhibited a monosigmoidal profile with  $pK_{app}$  values of  $5.2 \pm 0.1$  and  $6.1 \pm 0.1$  for the wild-type and the H66A <sup>h</sup>3-MSTs, respectively (Figure 4A). Thus, the moderate 0.9 unit-increase in the  $pK_{app}$  of the catalytic Cys shows that no significant change occurs around this residue upon substituting an alanine for His66, as supported by similar  $\epsilon_s$ -values (ie  $6180 \pm 160 \text{ M}^{-1} \cdot \text{cm}^{-1}$  vs  $6280 \pm 100 \text{ M}^{-1} \cdot \text{cm}^{-1}$ ). In an attempt to titrate the thiol group of 3-MP, the pH-dependence of the rate-constant associated with the first step of sulfur transfer was determined for the wild-type and H66A <sup>h</sup>3-MSTs, over a pH range of 4.5-10 and at 1 mM 3-MP, a saturating concentration for both enzymes ( $K_{3-MP} \sim 100 \text{ }\mu\text{M}$ ). Unexpectedly,  $k_{max1}$  values at pH 7.9 were approx. 3-fold higher than those determined in the presence of 50 mM Tris (see Table 1) for the wild-type and the H66A <sup>h</sup>3-MSTs, respectively. A similar stimulating effect due to the higher ionic strength of the polybuffer was observed for the bacterial enzyme, leading to rate-constant values predicted to be higher than  $4500 \text{ s}^{-1}$  at pH 8.0 for the wild-type <sup>Ec</sup>3-MST, and so above the technical limits of a stopped-flow apparatus. This explains why all pH-dependence studies were done on the human enzymes. The resulting pH- $k_{max1}$  curves exhibited sigmoidal profiles that were related to the contribution of one ionizable group of  $pK_{app}$   $5.9 \pm 0.1$  or  $8.3 \pm 0.1$  for the wild-type or the H66A <sup>h</sup>3-MST, respectively (Figure 4B). To assign the  $pK_{app}$  values one ought to consider whether they relate to the enzyme or the substrate because the pH-dependence of  $k_{max1}$  refers to the enzyme-substrate complex. In this pH range, the contribution of the carboxyl group of the substrate can be excluded as both Arg178 and Arg187 are likely to decrease its  $pK_{app}$  to a value much lower than 4.5. Therefore, the  $pK_{app}$ s 5.9 and 8.3 are due to ionization of the thiol

group of either the catalytic Cys237 or the 3-MP. Several lines of evidence argue for an assignment to the thiol group of the substrate. The closed  $k_{lim}$  values determined at optimal pH (ie  $385 \pm 5 \text{ s}^{-1}$  vs  $830 \pm 20 \text{ s}^{-1}$ , Figure 4B) indicate that, in the H66A <sup>h</sup>3-MST, the catalytic Cys237 and the 3-MP remain positioned such that an efficient sulfur transfer occurs towards the Cys237. As 3-MP is strongly anchored within the active site through stabilizing interactions with Arg178 and Arg187, the orientation of Cys237 relative to 3-MP is not modified, as well. Likewise, no drastic increase in the  $pK_{app}$  of Cys237 should be observed because the substitution H66A is expected to have the same impact on the conformation of the catalytic loop in the free and the complex forms. It was thus reasonable to assign the  $pK_{app}$  of 5.9 or 8.3 to the 3-MP thiol group. The strong decrease in its chemical reactivity at neutral pH suggests that substituting an Ala for His66 induces a movement of the catalytic loop that nearly abolishes the electrostatic contribution of the peptidic NH-groups in stabilizing the thiolate form and one can assume that the same is true when substituting Arg102. Altogether, this led us to propose a mechanism whereby the persulfide formation is mainly driven by electrostatic contributions provided by the catalytic loop (Scheme 5). The interactions Arg178/C<sub>2</sub>-C<sub>3</sub> and Arg187/C<sub>3</sub> permit an efficient positioning of the 3-MP with respect to the catalytic Cys237 that is already fully activated in the resting state. However, the nucleophilic attack undergone by the 3-MP thiol group critically depends on its deprotonation, which is favored by the electrostatic environment provided by the catalytic loop. Although this proposal agrees well with that based on QM/MM studies performed on the human enzyme,<sup>22</sup> a major difference emerges regarding the role ascribed to Ser239. Indeed, any key role of this residue in the activation of the 3-MP thiol group and thus in the sulfur transfer step can be ruled out, as clearly shown by our kinetic data (Table 1). Moreover, the fact that similar values of  $k_{max1}$  were obtained at pH 6.0 and pH 8.0 for the wild-type and the S239A <sup>h</sup>3-MSTs (data not shown) proves that no significant shift

in the  $pK_{\text{app}}$  of the 3-MP thiol group occurs upon substituting Ser239, thus providing additional support to our statement.

*A water molecule is required to protonate the pyruvate enolate* – To further decipher the mechanism whereby 3-MSTs catalyze the first step of the reaction, it was necessary to determine the way by which the methylene group of the enolate tautomer of pyruvate is protonated. Interestingly, the mutated H66N<sup>Ec</sup>3-MST exhibits kinetic properties identical to those of the wild type. Because an Asn side-chain is unable to abstract or donate protons, a proton relay involving the residues depicted to be part of the Ser/His/Asp triad can be excluded, in contrast to what was proposed in the literature.<sup>17,18,22</sup> It was thus reasonable to postulate that a water molecule was associated with this proton transfer process. To address this issue, SKIE were measured on the first step of sulfur transfer at pL 8.0 and substituting D<sub>2</sub>O for H<sub>2</sub>O resulted in a 2.2- and 2.5-fold decrease in  $k_{\text{max}1}$  for the bacterial and the human enzyme, respectively. The contribution of solvent-derived protons was further analyzed by performing proton inventory experiments for the wild-type <sup>h</sup>3-MST at pL 8.0. The normalized  $k_{\text{max}1}$  ( $k_n/k_0$ ) was plotted versus the D<sub>2</sub>O mole fraction ( $n$ ) and the data were fit to equation 6 (Figure 5) yielding a fractionation factor  $\Phi^{\text{T}}$  of  $0.44 \pm 0.05$ . The linearity of the plot accounts for a single solvent-derived proton in the rate-determining transition state and considering that  $k_{\text{max}1}$  values were obtained by monitoring the fluorescence changes upon going from the reduced to the persulfide forms, the protonation of the pyruvate enolate is thus concomitant to the persulfide formation. Therefore, and although it was excluded from the QM/MM studies,<sup>22</sup> our results suggest that a water molecule of the active site is the direct proton donor to pyruvate enolate as also proposed for the reactions catalyzed by pyruvate kinase and pyruvate class II aldolase.<sup>30,31</sup> Based on the crystal structure of the <sup>h</sup>3-MST that includes the

pyruvate substrate (PDB code: 4JGT), the best candidate seems to be the water W1 which could be held in position through an H-bond network involving the Thr242 side-chain.

## CONCLUSION

Our work provides significant insights on 3-MSTs catalysis and more specifically emphasizes the critical role of active site electrostatics in the formation of reactive cysteine persulfides. Through the contribution of its peptidic NH groups, the CGSGVT catalytic loop acts as a “thiolate hole” favoring the deprotonation of the 3-MP and Cys237 thiol groups required for a  $S^0$  transfer. In addition, the Arg178 and Arg187 guanidinium groups permit a productive binding of the substrate and further polarize the C-S bond, and the His66 and Arg102 side-chains anchors the catalytic loop through an H-bond network. Altogether, this delineates a pattern of interactions that permits a very efficient sulfur transfer between the substrate 3-MP and the catalytic Cys237. Furthermore, the water-mediated protonation of the pyruvate enolate is shown to be rate-determining for the  $S^0$  transfer and thus occurs concomitantly to the cysteine persulfide formation. In conclusion, the thiolate-based chemistry used by 3-MSTs is highly dependent on the CGSGVT catalytic loop and the critical role played by an active site loop seems to be a mechanistic feature common to other members of the rhodanese structural family, as already demonstrated for the so-called P-loop of the eukaryotic arsenate reductases and protein tyrosine phosphatases.<sup>32,33</sup>

## ASSOCIATED CONTENT

### Supporting Information

Figure S1- <sup>Ec</sup>3-MST and <sup>h</sup>3-MST sequence alignment and secondary structure comparison.

Figure S2- <sup>Ec</sup>3-MST mass spectrometry analyses.

Figure S3- <sup>Ec</sup>3-MST and <sup>h</sup>3-MST fluorescence spectra.

## AUTHOR INFORMATION

### Co-corresponding Authors

\* E-mail: [sandrine.boschi@univ-lorraine.fr](mailto:sandrine.boschi@univ-lorraine.fr) (S.B.M.), [francois.talfournier@univ-lorraine.fr](mailto:francois.talfournier@univ-lorraine.fr) (F.T.)

### Author Contributions

All authors have given approval to the final version of the manuscript.

## ACKNOWLEDGMENTS

This work was funded by the Région Lorraine and supported by the CNRS, the University of Lorraine and the Fédération de Recherche 3209 “Bioingénierie Moléculaire, Cellulaire et Thérapeutique”. J.C.L. was supported by the French Research Ministry. Mass spectrometry was performed at the “Service commun de spectrométrie de masse et des techniques chromatographiques couplées” from the University of Lorraine.

## ABBREVIATIONS

3-MST, 3-mercaptopyruvate sulfurtransferase; <sup>h</sup>3-MST, human 3-mercaptopyruvate sulfurtransferase; <sup>Ec</sup>3-MST, 3-mercaptopyruvate sulfurtransferase from *E. coli*; 3-MP, 3-

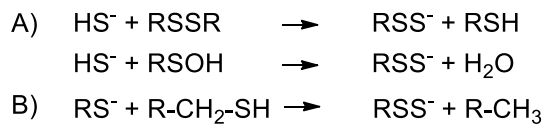
mercaptopyruvate; Trx, thioredoxin; TrxR, thioredoxin reductase; LDH, lactate dehydrogenase; SKIE, solvent kinetic isotope effect.

## REFERENCES

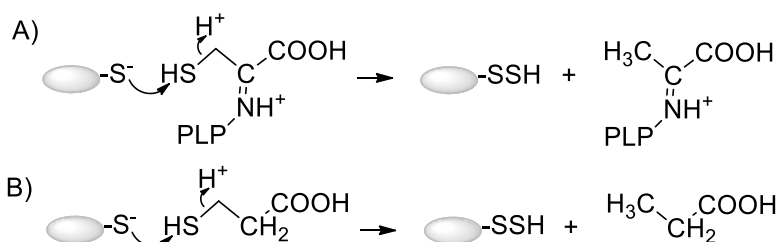
- (1) Mishanina, T. V.; Yadav, P. K.; Ballou, D. P.; Banerjee, R. *J. Biol. Chem.* **2015**, *290*, 25072-80.
- (2) Mueller, E. G. *Nat. Chem. Biol.* **2006**, *2*, 185-194.
- (3) Park, C. M.; Weerasinghe, L.; Day, J. J.; Fukuto, J. M.; Xian, M. *Mol. Biosyst.* **2015**, *11*, 1775-85.
- (4) Yadav, P. K.; Martinov, M.; Vitvitsky, V.; Seravalli, J.; Wedmann, R.; Filipovic, M. R.; Banerjee, R. *J. Am. Chem. Soc.* **2016**, *138*, 289-99.
- (5) Toohey, J. I. *Anal. Biochem.* **2011**, *413*, 1-7.
- (6) Ida, T.; Sawa, T.; Ihara, H.; Tsuchiya, Y.; Watanabe, Y.; Kumagai, Y.; Suematsu, M.; Motohashi, H.; Fujii, S.; Matsunaga, T.; Yamamoto, M.; Ono, K.; Devarie-Baez, N. O.; Xian, M.; Fukuto, J. M.; Akaike, T. *Proc. Natl. Acad. Sci. U. S. A.* **2014**, *111*, 7606-11.
- (7) Cuevasanta, E.; Lange, M.; Bonanata, J.; Coitino, E. L.; Ferrer-Sueta, G.; Filipovic, M. R.; Alvarez, B. *J. Biol. Chem.* **2015**, *290*, 26866-26880.
- (8) Cuevasanta, E.; Möller, M. N.; Alvarez, B. *Arch. Biochem. Biophys.* **2017**, *617*, 9-25.
- (9) Kessler, D. *FEMS Microbiol. Rev.* **2006**, *30*, 825-840.
- (10) Cavuzic, M.; Liu, Y. *Biomolecules* **2017**, *7*, E27.
- (11) Zheng, L.; White, R. H.; Cash, V. L.; Jack, R. F.; Dean, D. R. *Proc. Natl. Acad. Sci. U. S. A.* **1993**, *90*, 2754-8.
- (12) Zheng, L.; White, R. H.; Cash, V. L.; Dean, D. R. *Biochemistry* **1994**, *33*, 4714-20.
- (13) Colnaghi, R.; Cassinelli, G.; Drummond, M.; Forlani, F.; Pagani, S. *FEBS Lett.* **2001**, *500*, 153-6.
- (14) Westrop, G. D.; Georg, I.; Coombs, G. H. *J. Biol. Chem.* **2009**, *284*, 33485-33494.
- (15) Bordo, D.; Bork, P. *EMBO Rep.* **2002**, *3*, 741-6.
- (16) Cipollone, R.; Ascenzi, P.; Visca, P. *IUBMB Life* **2007**, *59*, 51-9.
- (17) Alphey, M. S.; Williams, R. A.; Mottram, J. C.; Coombs, G. H.; Hunter, W. N. *J. Biol. Chem.* **2003**, *278*, 48219-27.

- (18) Yadav, P. K.; Yamada, K.; Chiku, T.; Koutmos, M.; Banerjee, R. *J. Biol. Chem.* **2013**, *288*, 20002-20013.
- (19) Mikami, Y.; Shibuya, N.; Kimura, Y.; Nagahara, N.; Ogasawara, Y.; Kimura, H. *Biochem. J.* **2011**, *439*, 479-485.
- (20) Nagahara, N.; Nishino, T. *J. Biol. Chem.* **1996**, *271*, 27395-401.
- (21) Spallarossa, A.; Forlani, F.; Carpen, A.; Armirotti, A.; Pagani, S.; Bolognesi, M.; Bordo, D. *J. Mol. Biol.* **2004**, *335*, 583-93.
- (22) Huang, G. T.; Yu, J. S. K. *J. Phys. Chem. B* **2016**, *120*, 4608-4615.
- (23) Mössner, E.; Huber-Wunderlich, M.; Glockshuber, R. *Protein Sci.* **1998**, *7*, 1233-44.
- (24) Mulrooney, S. B.; Williams, C. H. Jr. *Protein Sci.* **1997**, *6*, 2188-95.
- (25) Cook, P. F., Ed. *Enzyme mechanism from isotope effects* **1991**, CRC Press, Boca Raton, Florida .
- (26) Rabin, B. R. *Biochem. J.* **1967**, *102*, 22C-23C.
- (27) Frieden, C. *Annu. Rev. Biochem.* **1979**, *48*, 471-89.
- (28) Antoine, M.; Boschi-Muller, S.; Branlant, G. *J. Biol. Chem.* **2003**, *278*, 45352-7.
- (29) Talfournier, F.; Colloc'h, N.; Mornon, J. P.; Branlant, G. *Eur. J. Biochem.* **1998**, *252*, 447-57.
- (30) Susan-Resiga, D.; Nowak, T. *J. Biol. Chem.* **2003**, *278*, 12660-71.
- (31) Coincon, M.; Wang, W.; Sygusch, J.; Seah, S.Y. K. *J. Biol. Chem.* **2012**, *287*, 36208-21.
- (32) Bhattacharjee, H.; Sheng, J.; Ajees, A.A.; Mukhopadhyay, R.; Rosen, B.P. *Biochemistry* **2010**, *49*, 802-809.
- (33) Zhang, Z.Y. *Prog. Nucl. Res. Molec. Biol.* **2003**, *73*, 171-220.

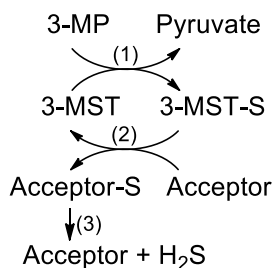
## SCHEMES



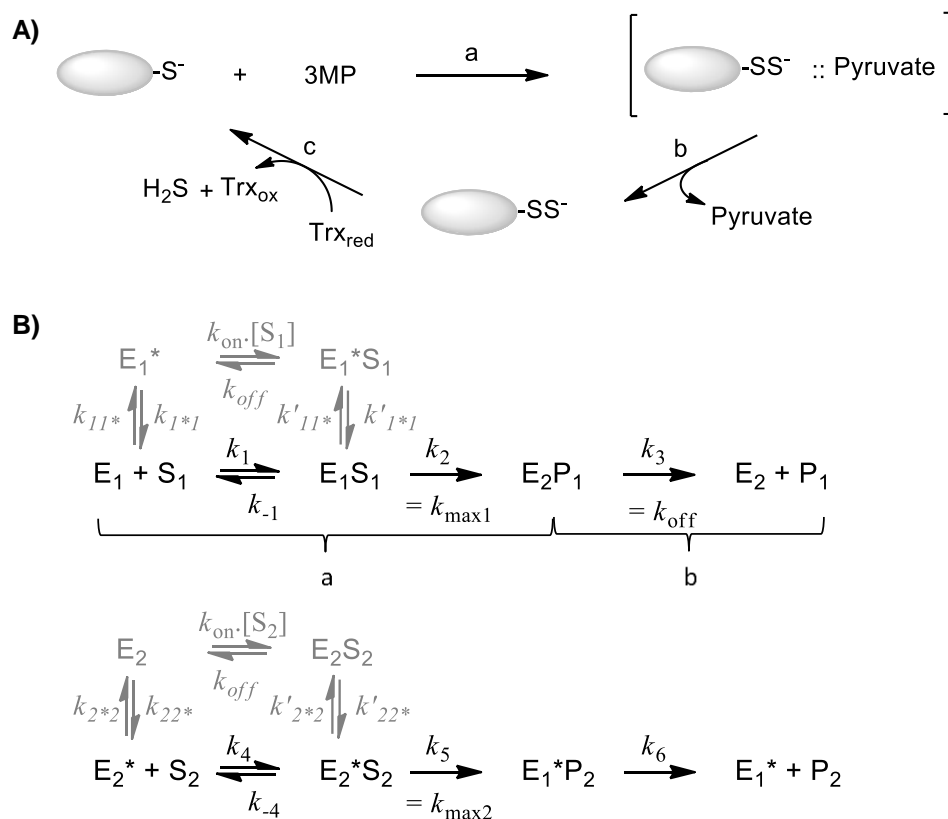
**Scheme 1: Mechanism of persulfide formation from hydrogen sulfide and oxidized thiol (A) or sulfur compound and reduced thiol (B).**



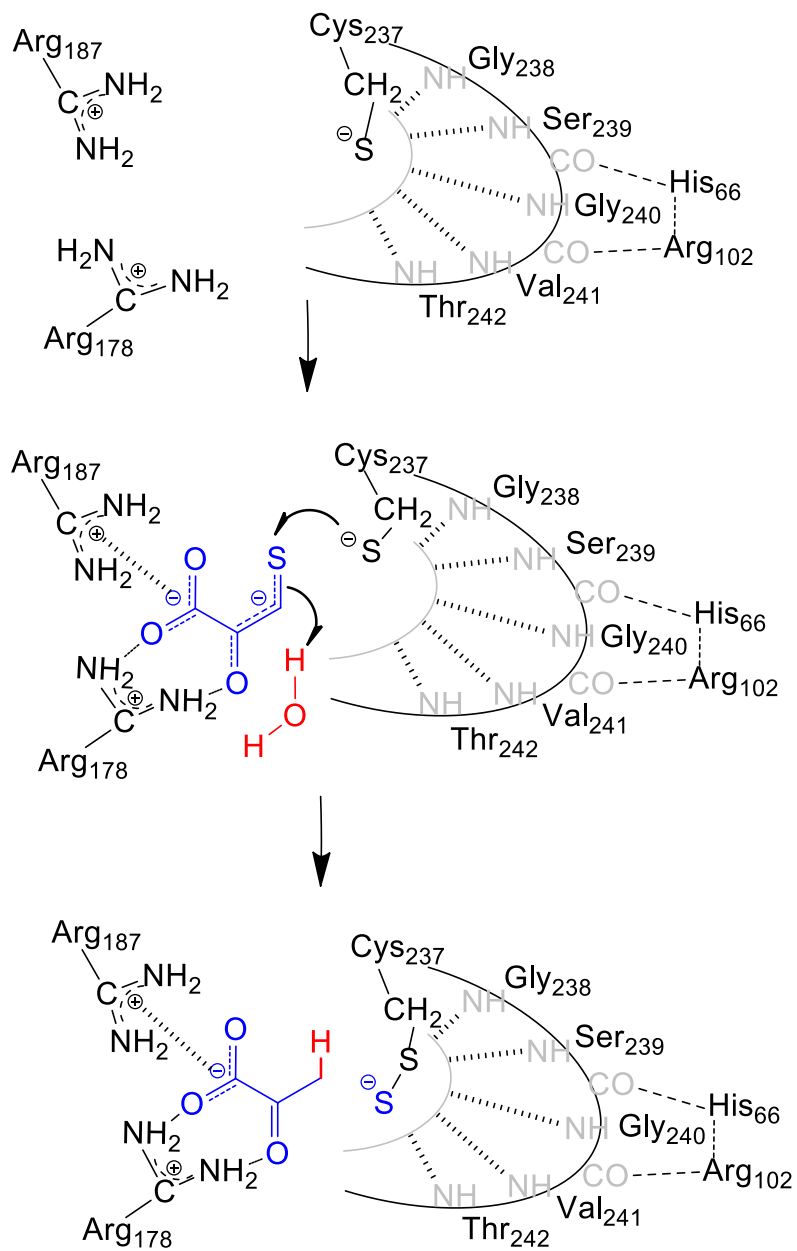
**Scheme 2: Mechanism of persulfide formation catalyzed by cysteine desulfurase (A) or thioltransférase (B).**



**Scheme 3: 3-MST-dependent reactions leading to H<sub>2</sub>S production. The sulfur atom is first transferred from 3-MP to 3-MST (1) leading to formation of a persulfide intermediate (3-MST-S), then from 3-MST-S to an acceptor substrate (2). If the reaction product (Acceptor-S) is under persulfide form, its decomposition leads to the formation of H<sub>2</sub>S (3).**



**Scheme 4:** Scheme of the Trx-dependent reaction (A: a, persulfide formation; b, pyruvate release; c, disulfide oxidized Trx formation); and proposed kinetic model for the 3-MST-catalyzed reaction (B: S<sub>1</sub>, 3-MP; S<sub>2</sub>, Trx; P<sub>1</sub>, pyruvate and P<sub>2</sub>, persulfide Trx; E<sub>1</sub>/E<sub>1</sub>\* and E<sub>2</sub>/E<sub>2</sub>\*, thiol and persulfide 3-MSTs, respectively).



**Scheme 5: Proposed catalytic mechanism of persulfide 3-MST formation.**

## FIGURES

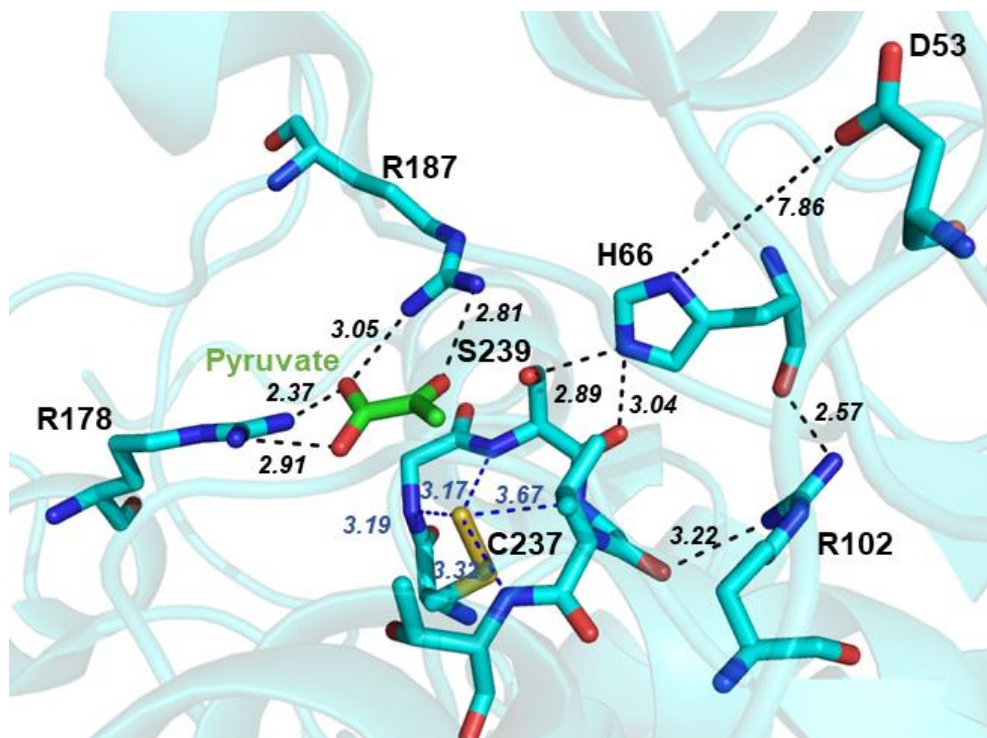


**Figure 1:** Active site of persulfurated <sup>h</sup>3-MST in complex with pyruvate (PDB code 4JGT). The sulfur atoms of the catalytic Cys237 are colored yellow and the figure was generated using PyMOL ([www.pymol.org](http://www.pymol.org)).

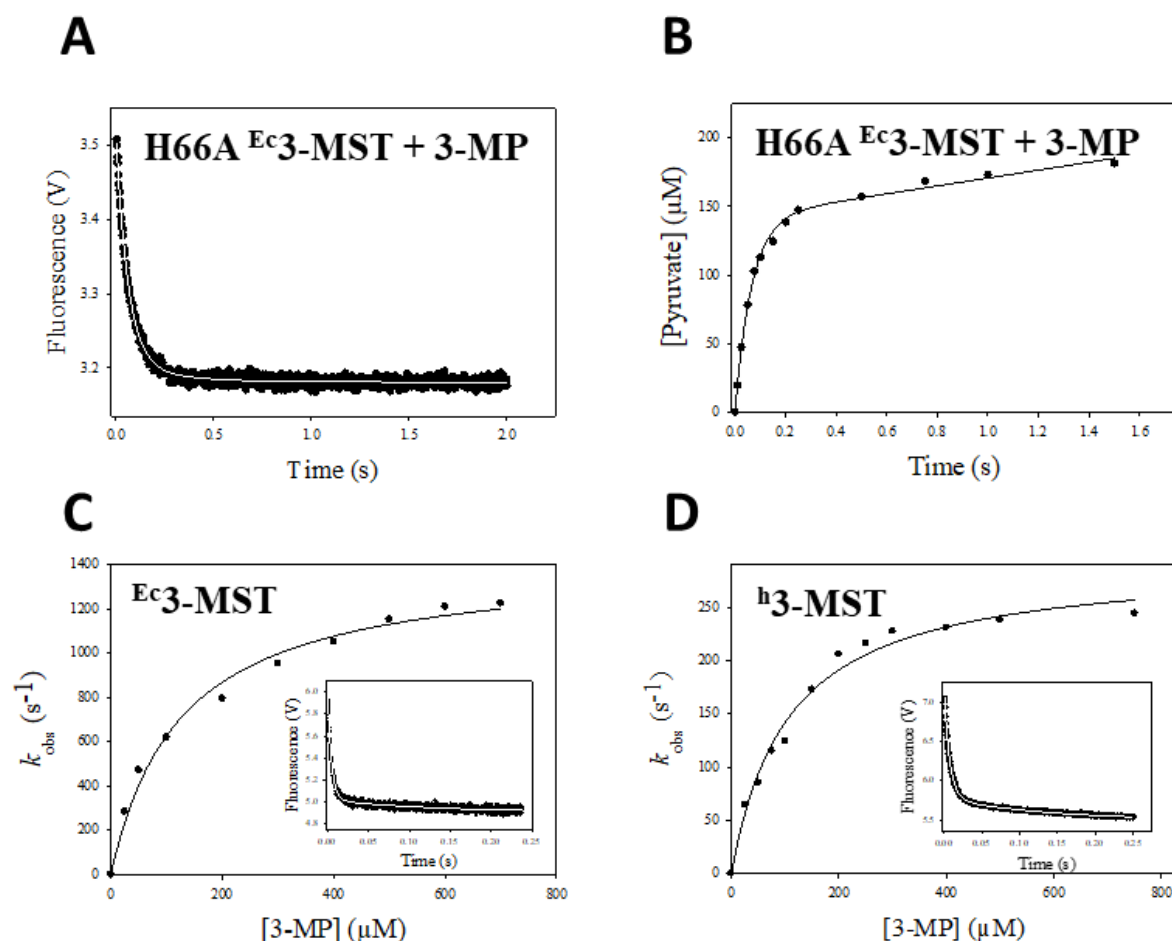


**Figure 2: Kinetics of the first step of sulfur transfer under single turn-over conditions.**

(A) The change in fluorescence intensity of 5 μM H66A <sup>Ec3</sup>-MST was monitored after mixing with 2 mM 3-MP and experimental data were fit to a monophasic expression (white line). (B) Time-resolved appearance of pyruvate for H66A <sup>Ec3</sup>-MST: experimental data were fit to equation 1. (C) and (D) Determination of the catalytic parameters for <sup>Ec3</sup>-MST and <sup>h3</sup>-MST, respectively, using the fluorescence-based approach. The experimental data were fit to equation 2 and the insets show representative transients obtained in the presence of 100 μM 3-MP.

The experiments were carried out three times independently and standard error on each experimental point was less than 5%.

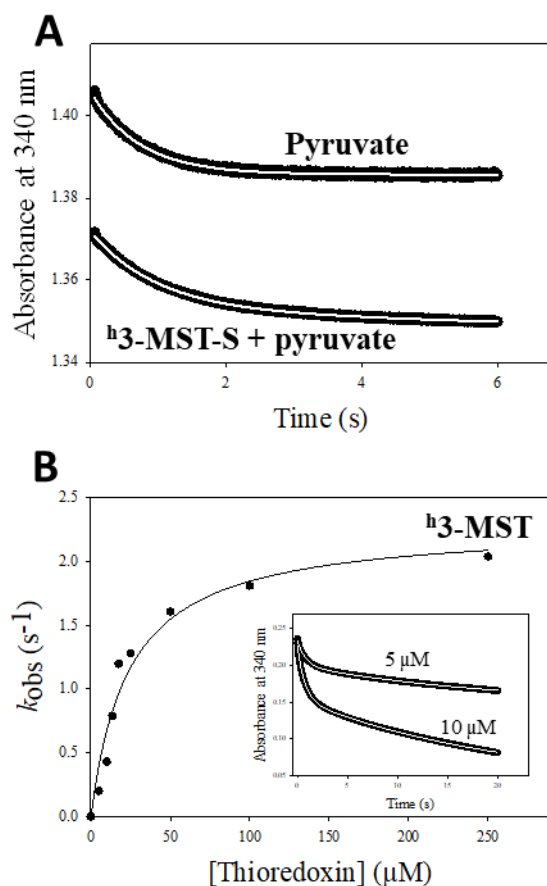


**Figure 3: Kinetics of pyruvate dissociation from the persulfide  $^h3\text{-MST}$  / pyruvate complex (A) and of sulfur transfer from persulfide  $^h3\text{-MST-S}$  to Trx (B).**

(A) Time-dependent decrease in  $A_{340}$  after mixing persulfide  $^h3\text{-MST}$  ( $^h3\text{-MST-S}$ ) and pyruvate in the presence of LDH/NADH as pyruvate-trapping system. The collected data were fit to a monophasic expression in the absence of  $^h3\text{-MST-S}$  (upper trace, white line) and to a biphasic expression in the presence of  $^h3\text{-MST-S}$  (lower trace, white line).

(B) Determination of the catalytic parameters for the sulfur transfer from  $^h3\text{-MST-S}$  to Trx by using the TrxR/NAPDH regeneration system. The experimental data were fit to equation 4. The inset corresponds to representative transients obtained by mixing 5 or 10  $\mu\text{M}$   $^h3\text{-MST-S}$  with 50  $\mu\text{M}$  Trx. The traces were fit to a biphasic expression (white line).

The experiments were carried out two times independently and standard error on each experimental point was less than 5%.

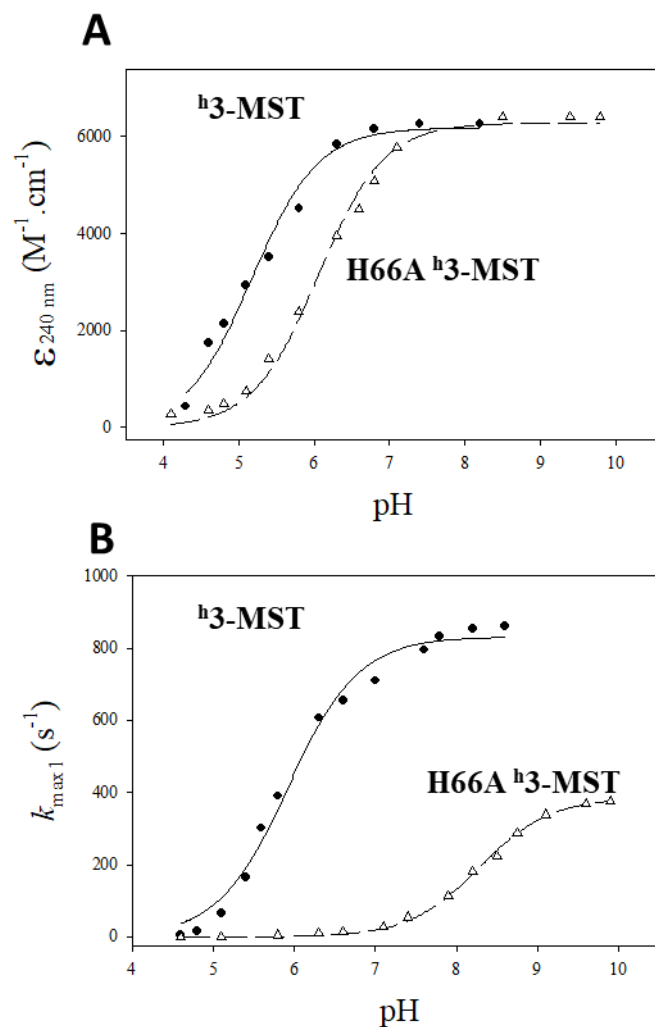


**Figure 4: pH-dependence of the absorbance properties of the catalytic Cys237 (A) and of the rate-constant  $k_{\text{max}1}$  (B) for the wild-type (●) and H66A (Δ) h3-MSTs.**

(A) The pH-dependent ionization of the Cys237 was monitored by the thiolate-specific absorbance at 240 nm over a pH range 4 to 10 in polybuffer A. Experimental data were fit to equation 5.

(B) pH-dependence of the rate constant  $k_{\text{max}1}$  associated with the first step of sulfur transfer. The  $k_{\text{max}1}$  values were determined using the fluorescence-based approach over a pH range 4.5 to 10 in polybuffer A and data were fit to equation 3.

The experiments were carried out two times independently and standard error on each experimental point was less than 5%.

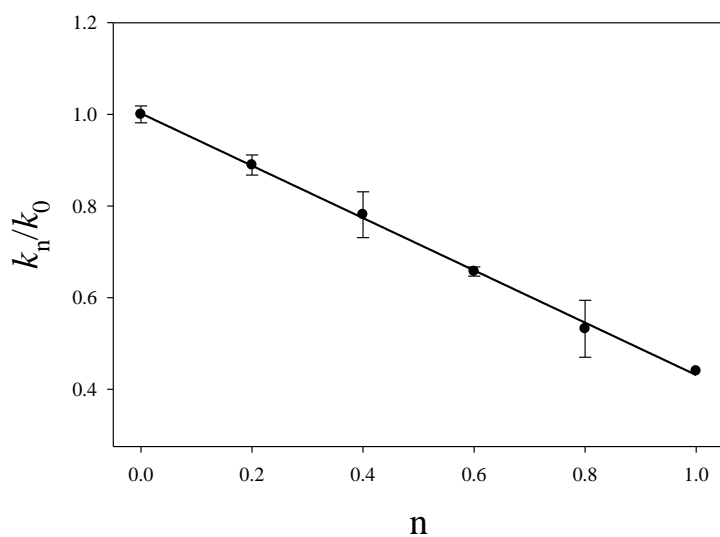


**Figure 5:** Proton inventory for the first step of sulfur transfer catalyzed by  $^3\text{H}$ -MST at pL 8.0. The normalized  $k_{\text{max}1}$  ( $k_n/k_0$ ) is plotted against the  $\text{D}_2\text{O}$  mole fraction  $n$ . The line represents the best fit of the data to Equation 6. Experiments were carried out three times independently.

TABLE

**Table 1: Kinetic parameters of the sulfur transfer steps and of the overall reaction for wild-type 3-MSTs and the different mutants.**

	<i>Sulfur transfer</i>		<i>Steady-state</i>	
	$k_{\max 1}$ (s <sup>-1</sup> )	$K_{3\text{-MP}}$ (μM)	$k_{\text{cat}}$ (s <sup>-1</sup> )	$K_{\text{M (3-MP)}}$ (mM)
<i>E<sub>c</sub></i> 3-MST				
wild-type	1520 ± 90	160 ± 30	112 ± 5	1.0 ± 0.1
D53A	460 ± 60	25 ± 7	1.0 ± 0.1	2.4 ± 0.1
H66A	25 ± 1	110 ± 10	20 ± 1	0.43 ± 0.06
H66N	1260 ± 90	80 ± 20	75 ± 5	1.4 ± 0.2
R102L	40 ± 1	300 ± 50	49 ± 3	0.9 ± 0.2
R102K	52 ± 5	100 ± 30	59 ± 3	1.0 ± 0.2
H66A / R102L	3.9 ± 0.1	70 ± 10	3.9 ± 0.2	1.0 ± 0.2
R178L	21 ± 1	100 ± 20	0.05 ± 0.01	15 ± 3
R187L	350 ± 80	(15 ± 6)·10 <sup>3</sup>	0.16 ± 0.02	4 ± 1
R178L / R187L	0.5 ± 0.1	200 ± 10	0.068 ± 0.003 <sup>a</sup>	23 ± 2 <sup>f</sup>
S239A	960 ± 70 <sup>b</sup>	620 ± 90	2.5 ± 0.1 <sup>c</sup>	0.24 ± 0.02 <sup>f</sup>
<i>h</i> 3-MST				
wild-type	290 ± 10	110 ± 10	0.47 ± 0.05 <sup>d</sup>	1.7 ± 0.1 <sup>f</sup>
H66A	31 ± 1	120 ± 10	0.48 ± 0.03	0.79 ± 0.16
S239A	340 ± 20	870 ± 130	0.11 ± 0.01 <sup>e</sup>	0.6 ± 0.05 <sup>f</sup>

<sup>a,b,c,d,e</sup> Parameters obtained by fitting the experimental data to the Hill equation with n values of 1.7 ± 0.2<sup>a</sup>, 3.5 ± 0.3<sup>b</sup>, 3 ± 0.6<sup>c</sup>, 1.7 ± 0.1<sup>d</sup> and 2 ± 0.3<sup>e</sup>. <sup>f</sup>  $K_{0.5}$  values.

TOC graphic

